Spin-Polarized Semiconducting Band Structure of Monolayer Graphene on Ni(111)

Yu Zhang,[1,†] Xuelei Sui,[2,†] Dong-Lin Ma,[1] Ke-Ke Bai,[1] Wenhui Duan,[2] and Lin He[1,*]

[1] *Center for Advanced Quantum Studies, Department of Physics, Beijing Normal University, Beijing 100875, People's Republic of China*

[2] *State Key Laboratory of Low-Dimensional Quantum Physics and Collaborative Innovation Center of Quantum Matter, Department of Physics, Tsinghua University, Beijing 100084, People's Republic of China*

(Received 13 July 2018; revised manuscript received 11 September 2018; published 19 November 2018)

The magnetic properties of graphene have attracted much attention for more than a decade. Recent studies have shown that adatoms or atomic vacancies in graphene could exhibit localized magnetic moments. However, a macroscopic spin-polarized semiconducting band structure has never been experimentally realized in graphene. Here, we demonstrate that a graphene monolayer, hybridized with an underlying Ni(111) substrate, exhibits a spin-polarized semiconducting state even at room temperature. Our spin-polarized scanning tunneling microscopy (STM) experiments, complemented by first-principles calculations, explicitly demonstrate that the interaction between graphene and the Ni substrate generates a large gap in graphene and simultaneously leads to a relative shift between majority- and minority-spin bands. Consequently, the graphene sheet on the Ni substrate exhibits a spin-polarized gap with an energy of several tens of meV even at room temperature.

DOI: 10.1103/PhysRevApplied.10.054043

I. INTRODUCTION

Pristine graphene is a diamagnetic semimetal [1]. The realization of magnetism in graphene has attracted much attention over the years, since the *s–p* electron magnetism is predicted to be stable even at high temperatures. Recently, many groups have attempted to introduce magnetism in graphene [2–13]. For example, it has been demonstrated that graphene with atomic defects and hydrogen chemisorption defects could exhibit localized magnetic moments. However, due to the difficulty of controlling the densities and the regular arrangement of the defects, it is almost impossible to realize a macroscopic spin-polarized semiconductor band structure by simply introducing adatoms or atomic vacancies. To overcome this difficulty, we report a method with which to achieve this goal by introducing a magnetic substrate Ni(111), which can drive the graphene monolayer to exhibit a spin-polarized semiconducting band structure. Once you have a synthesized-graphene monolayer on a Ni(111) substrate, the π band of graphene is strongly perturbed by the *d* electrons of Ni. The π-*d* interaction not only opens up a gap of several hundred meV in graphene, but also lifts the degeneracy of majority- and minority-spin bands around the *K* point of graphene due to the exchange-splitting effect [14–16], thus realizing the spin-polarized ferromagnetic semiconducting state with a gap of tens of meV in graphene. The local magnetic moments of atomic defects in graphene and the edge magnetism in individual zigzag graphene nanoribbons are studied successfully by measuring their electronic structures via scanning tunneling microscopy (STM) [2–5,7–9]. Here, we use spin-polarized STM measurements for the first time to directly measure both the relative energy shift between the majority- and minority-spin bands and the gap opening of the graphene monolayer on the Ni(111) substrate. These results provide clear evidence of the emergence of the spin-polarized semiconducting band structure in the graphene monolayer.

II. EXPERIMENTAL RESULTS AND DISCUSSION

A. Graphene monolayer on a Ni(111) single crystal

The graphene monolayer is grown on a Ni(111) single crystal (5×5 mm^2 area, 1-mm thickness) via a traditional low-pressure chemical-vapor deposition (LPCVD) method [17–19] (the growth process is schematically shown in Fig. S1 [20]). The thickness of the as-grown graphene is characterized by Raman spectra measurements. Figure 1(a) shows typical Raman spectra measured at different positions of the synthesized graphene transferred to a 300-nm

*helin@bnu.edu.cn

†These authors contributed equally to this work.

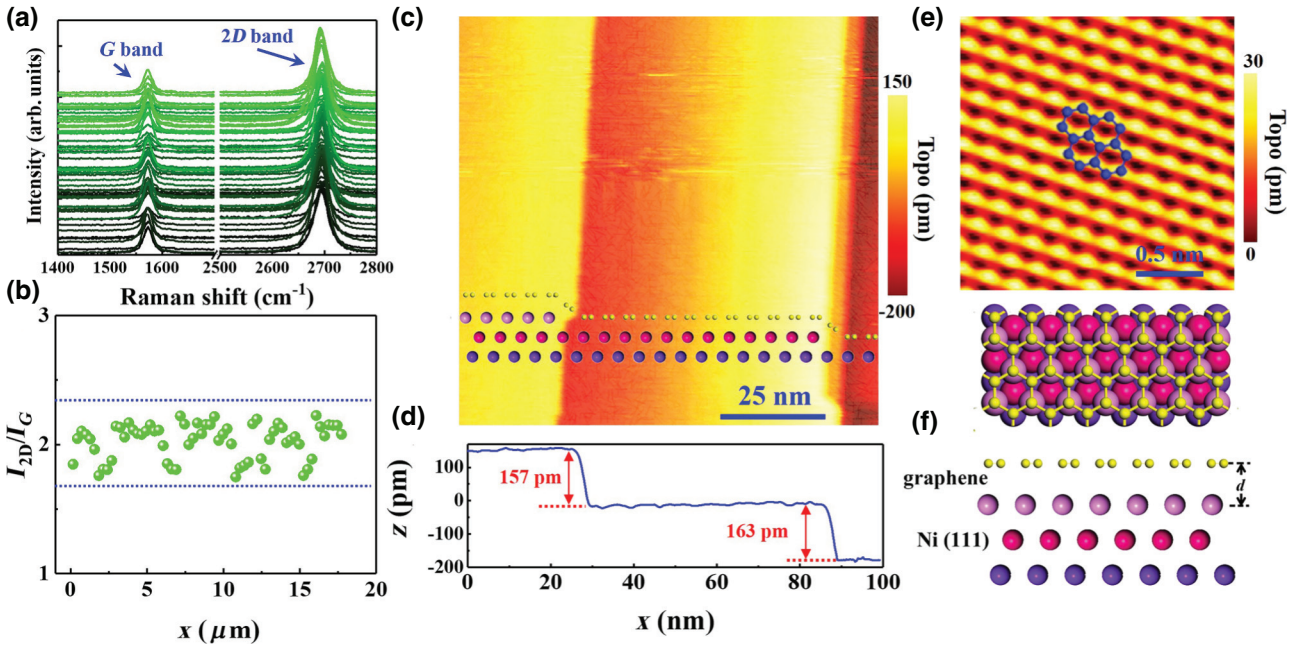

FIG. 1. (a) Raman spectra of graphene transferred to a 300-nm SiO_2/Si substrate measured at different positions. (b) The ratios of the intensities of the 2D band and G band vary with the recorded positions. (c) 100×100 nm^2 STM image of graphene monolayer across typical monatomic Ni(111) steps ($V_b = 0.5$ V, $I = 0.2$ nA). (d) The height profile along the monatomic Ni(111) steps in c. (e) Zoom-in atomic-resolution STM image of graphene, showing the triangular lattice of the monolayer graphene on the Ni(111) surface. (f) Schematic image of a graphene monolayer on Ni(111) surface. The carbon atoms of the *A* sublattice are on top of the Ni atoms of the topmost atomic layer, while the atoms of the *B* sublattice are located above the hollow sites of the Ni(111) topmost layer.

SiO_2/Si substrate. Two peaks at 1580 and 2700 cm^{-1} in the Raman spectra are the *G* band and 2*D* band, respectively, which are the characteristic Raman peaks of graphene [17–19,21]. We can identify the layer number of graphene by comparing the intensities of the *G* band and the 2*D* band. Figure 1(b) shows the values of I_{2D}/I_G with an average value of about 2, indicating that the obtained sample under the growth process is mainly a graphene monolayer. Such a result is further confirmed by our STM measurements. Figures 1(c) and 1(d) show a representative STM topographic image of the graphene monolayer across typical monatomic Ni(111) steps. The widths of the Ni(111) terraces vary from about 20 nm to about 80 nm. As shown in Fig. 1(e), the atomic-graphene lattice can be resolved on the terraces, exhibiting a large intensity imbalance between the *A* and *B* sublattices. This indicates the inversion symmetry breaking of graphene by the substrate. For graphene on the Ni(111) surface [Fig. 1(f)], the carbon atoms of the *A* sublattice are mainly on top of the Ni atoms of the topmost atomic layer, while the atoms of the *B* sublattice are mainly located above the hollow sites of the topmost atomic layer of Ni due to their minor lattice mismatch. The strong chemical interaction between graphene and the Ni substrate not only results in the large sublattice asymmetry, but also dramatically changes the electronic band structure of graphene.

B. The gap of a graphene monolayer on a Ni(111) single crystal

Figure 2(a) shows several representative scanning tunneling spectroscopy (STS) spectra of the graphene monolayer on the Ni(111) surface recorded at different temperatures. It is interesting to note that we clearly observe a finite gap of approximately 40 meV in the graphene monolayer at low temperature. The STS spectra recorded at different positions (*A* atoms, *B* atoms, or in the hollow of the graphene lattice) have no obvious differences in our experiments. With increasing temperature, the gap feature in the STS spectra becomes weak due to thermal broadening. However, we still can detect the gaplike feature even at room temperature (300 K). Our experiment demonstrates that the main features of the STS spectra measured at different terraces (and at different positions) are almost the same regardless of the width of the terraces (see Fig. S2 [20]). Similar spectra are obtained with several different nonmagnetic-STM tips [Pt(80%)Ir(20%) tips], which removes any possible artificial effects as the origin of the observed result. The approximately 40 meV gap,

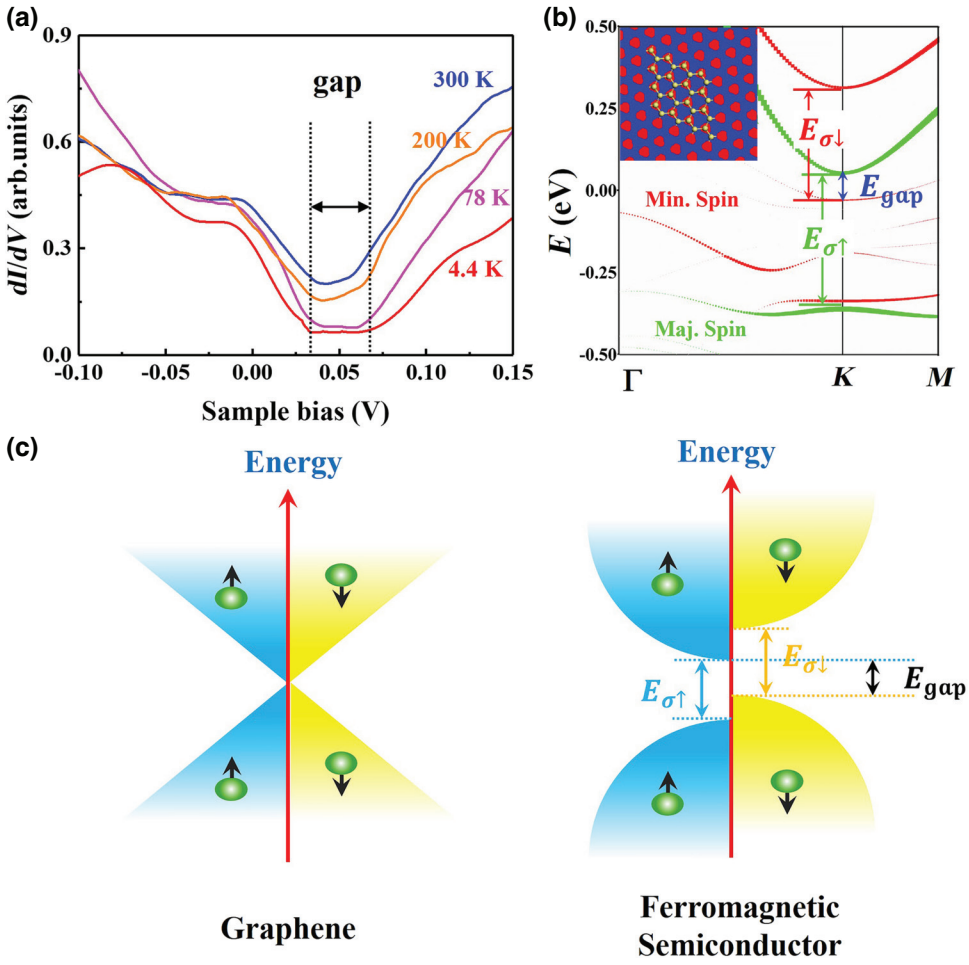

FIG. 2. (a) Representative STS spectra of the graphene on the Ni(111) surface recorded at different temperatures. (b) Band structures of graphene monolayer on the Ni(111) surface. The sizes of the dots represent the proportion of graphene orbits to the total orbits. The Fermi level is at zero energy. The labels Maj. Spin and Min. Spin indicate the majority-spin bands (green lines) and minority-spin bands (red lines) of the graphene monolayer on Ni(111), respectively. Inset: density functional theory (DFT)-simulated STM image of the graphene monolayer on the Ni(111) surface. (c) (Left) Low-energy electronic-band structure of graphene monolayer. The electronic structures for the spin-up and spin-down states are degenerate. (Right) Schematic-band structure of the ferromagnetic semiconductor.

which is asymmetric with respect to the Fermi level, helps us to eliminate the attribution of the phonon-mediated tunneling to the gap (approximately 120 meV) as its origin [22–24]. Moreover, we can also eliminate the biased-graphene bilayer as the origin of the observed gap based on the following reasons. First, our Raman spectra confirm that the studied sample is a graphene monolayer. Second, there are two low-energy asymmetrical peaks in the tunneling spectra of the gapped-graphene bilayer, which are generated at the valence-band edge and conduction-band edge of the gapped bilayer [25,26]. Obviously, such a feature is absent in our experiment. Third, the gap for the biased-graphene bilayer should be the same for nonmagnetic and spin-polarized STM measurements, which is quite different from our experimental results.

To further explore the origin of the observed gap, we carry out similar STS measurements on bare Ni(111) (see Fig. S3 [20]). The distinct spectra recorded for bare Ni(111) remove the electronic states of Ni(111) as the origin of the observed gap in Fig. 2(a). Simultaneously, we also measure STS spectra on an insulating hexagonal-boron nitride (*h*-BN) monolayer on Cu foil for comparison. In the *h*-BN/Cu system, we clearly observe the large band gap of approximately 5.9 eV for the *h*-BN monolayer (see Fig. S4 [20]). This indicates that the STM can predominantly probe the electronic states of the topmost monolayer underneath the STM tip, and the observed gap in Fig. 2(a) mainly reflects the electronic structure of the graphene monolayer on the Ni(111) surface [14,27]. The Ni(111) surface should play a vital role in the emergence of the gap in graphene, because the graphene monolayer on other metallic substrates, such as Cu [8,28–30], usually exhibits V-shaped spectra and there is no measurable band gap (see Fig. S5 [20]), as one would expect to observe for the pristine graphene monolayer.

The observation of a finite gap in the graphene monolayer on the Ni(111) surface is quite reasonable since the substrate generates enormous sublattice asymmetry in graphene [Fig. 1(e)], which is expected to open a gap in it [31–33]. However, with consideration of the strong chemical interaction between graphene and Ni and the observed large sublattice imbalance in graphene, the obtained gap of approximately 40 meV in the graphene monolayer [Fig. 2(a)] is unexpectedly small. The observed gap is only comparable to the expected gap for a graphene monolayer on a *h*-BN substrate [32,33], whereas the interaction

between graphene and *h*-BN is much weaker than that between graphene and Ni. To fully understand the electronic structure of the graphene monolayer on the Ni(111) surface, we carry out first-principles calculations on this system [34–37]. Figure 2(b) shows a representative theoretical electronic band structure of the studied system. The sizes of the dots represent the proportion of graphene orbits to the total orbits, and the largest proportion occurring at the K point is approximately 0.37 (see Fig. S6 [20]). Since the STM measurements predominantly probe the electronic states of the topmost graphene sheet, we only need to care about the band structure of graphene *C* orbits. The inset of Fig. 2(b) shows the calculated STM image of the graphene monolayer on the Ni(111) surface. Obviously, the strong chemical interaction between graphene and the Ni substrate results in the enormous sublattice asymmetry in graphene, as observed in our experiment. The enormous sublattice asymmetry generates a large gap (approximately 300 meV) in graphene, labeled $E_{\sigma\uparrow}$ and $E_{\sigma\downarrow}$ for the spin-up and spin-down electrons, respectively. Importantly, the strong π-d interaction between graphene and Ni not only opens up a large gap in graphene, but also lifts the degeneracy of the majority- and minority-spin bands around the *K* point of graphene, as shown in Fig. 2(b). Here, we should point out that the band edge of the minority band may also arise from electrons at the Γ point, since the energies of the minority valence band at the Γ point and the *K* point are similar, and tunneling from states at the Γ point is expected to be more probable in STM measurements [22–24]. According to our calculation, the spin splitting of graphene's conduction band is about 250 meV (similar to that for the valence band). The coexistence of the two effects (the gap opening and the spin splitting) induced by the Ni(111) substrate leads to the realization of the spin-polarized ferromagnetic semiconducting state with a gap of several tens of meV in graphene, as schematically shown in Fig. 2(c), which agrees well with our observations in the experiment. Since we observe the gap even at room temperature, our results, therefore, indicate that the graphene monolayer on the Ni(111) surface is the room-temperature ferromagnetic semiconductor. Very recently, x-ray magnetic circular-dichroism experiments [38] and spin-polarized surface-positronium spectroscopy [39] also pointed out that the graphene/Ni(111) system can lead to magnetic moments in the carbon atoms of the graphene monolayer.

C. The spin-polarized gap of graphene on a Ni(111) single crystal

To further confirm the ferromagnetic semiconducting state of the graphene on the Ni(111) surface, we carry out spin-polarized STM measurements, which provide us with unprecedented opportunities to further identify the

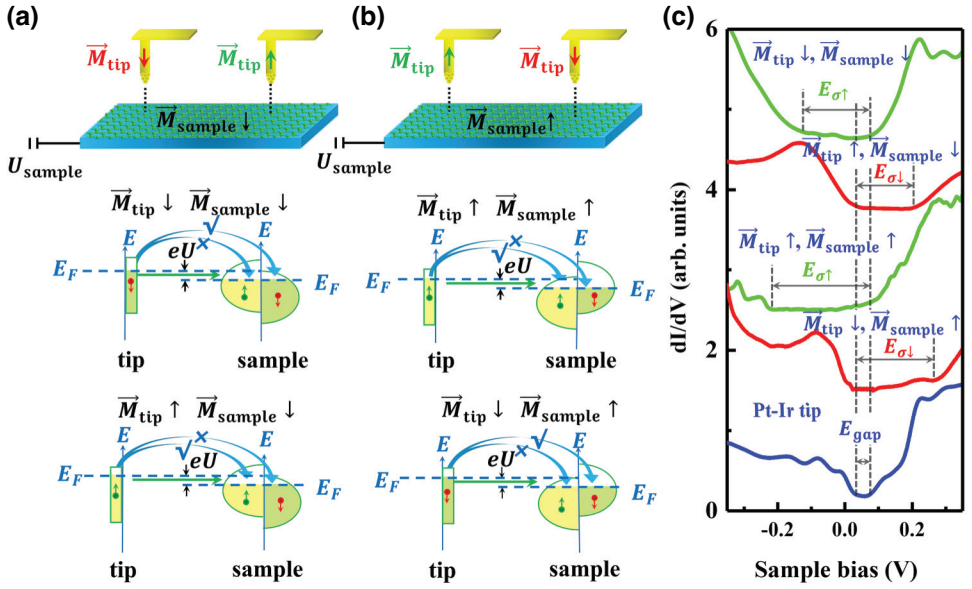

FIG. 3. (a),(b) Top panel: schematic experimental set up of spin-polarized STM. Spins of the sample aligned perpendicular to the sample surface can be detected by the Ni tip along the tip axis. Bottom panels: principle of spin-polarized tunneling between magnetic electrodes that exhibit a parallel ($\vec{M}_{tip}\downarrow, \vec{M}_{sample}\downarrow$ or $\vec{M}_{tip}\uparrow, \vec{M}_{sample}\uparrow$) and an antiparallel ($\vec{M}_{tip}\uparrow, \vec{M}_{sample}\downarrow$ or $\vec{M}_{tip}\downarrow, \vec{M}_{sample}\uparrow$) magnetization. The spin is conserved during the elastic-electron tunneling. (c) Spin-polarized *dI/dV* spectra of the graphene monolayer on the Ni surface. The red curve is measured when the tip polarization $\vec{M}_{tip}$ and the magnetization of the sample $\vec{M}_{sample}$ are antiparallel, which reflects the LDOS of the spin-down electrons. The green curve is measured when the $\vec{M}_{tip}$ and $\vec{M}_{sample}$ are parallel, which reflects the LDOS of the spin-up electrons. The blue dots are the *dI*/*dV* spectrum of graphene on the Ni(111) surface measured via a nonmagnetic Pt/Ir tip.

origin of the gap by separately detecting the majority- and minority-spin bands of graphene (Fig. 3) [40,41]. In our experiment, we use electrochemically-etched Ni tips (see Figs. S7 and S8 [20]) as the spin-polarized tips [42]. Due to the weak magnetocrystalline anisotropy of Ni [43], the magnetic polarization of the tip is always along the STM tip, i.e., perpendicular to the surface of the sample, due to the shape anisotropy of the STM tip. Before the STM measurements, a magnetic field of $B = 2.0$ T ($B = -2.0$ T) perpendicular to the surface of the sample is applied and then gradually removed to obtain an up-polarized (down-polarized) STM tip. After that, a magnetic field $B = -0.02$ T, which is much smaller than the reversal field of the tip that usually ranges from about 200 to 300 mT in our experiments, is applied on the sample to make sure that the spins of the sample are down-polarized. As a consequence, the magnetizations of the STM tip and the sample are either parallel or antiparallel, as shown in Fig. 3(a). A similar method can be adopted to make sure the spins of the sample are up-polarized by using a magnetic field of $B = 0.02$ T, as shown in Fig. 3(b). Because of the spin conservation during the elastic-electron tunneling, we can detect the spin-up and spin-down bands of graphene separately, as schematically shown in Fig. 3. In the case where the magnetizations of the STM tip and the sample are parallel, the measured tunneling spectrum mainly reflects the local density-of-state (LDOS) of the spin-up electrons in the sample. In the other case where the magnetic polarizations of the tip and the sample are antiparallel, the recorded dI/dV spectrum is primarily contributed by the LDOS of the spin-down electrons in the sample. For simplicity, the above discussion is based on the assumption that the STM tip is 100% spin polarized.

Figure 3(c) shows four representative spin-resolved dI/dV spectra of the graphene monolayer on Ni(111) probed according to the above method (see Figs. S9–S12 for more experimental results [20]). The spectra marked by green lines are measured when the spin polarizations of the tip and the sample are parallel, and the spectra marked by red lines are recorded when they are antiparallel. Very similar spectra have been obtained and verified by using several different Ni tips in our experiment. Additionally, we also rule out the DOS contributions of the underneath Ni(111) substrate [44] by directly measuring the STS spectra on bare Ni(111) with a spin-polarized Ni tip (see Fig. S13 [20]). The spin-polarized spectra recorded in the graphene monolayer on the Ni(111) surface exhibit quite large gaps of 200 to 300 meV, indicating that the strong interaction between graphene and the Ni substrate really generates large gaps, $E_{\sigma\uparrow}$ and $E_{\sigma\downarrow}$, for both the spin-up and spin-down electrons in the graphene. Moreover, there is quite a large shift between the charge neutrality points of the spin-up and spin-down bands. The overlap between the $E_{\sigma\uparrow}$ and $E_{\sigma\downarrow}$ is much smaller than the gaps for either the spin-up or spin-down electrons. As a consequence, we can only detect a gap of several tens of meV in graphene by using the nonmagnetic STM tip, as shown in Fig. 3(c). We can also rule out other mechanisms of inducing a spin-polarized energy band in the graphene-Ni system [15,16,45–47]. For example, the lattice deformations of graphene can be ruled out by carefully analyzing the STM image, and the Rashba Δ_{SO} of graphene on Ni is much smaller than the measured gap in our experiment. More theoretical analyses and discussions about the band gap of graphene are given in the Appendix. Our experimental result explicitly demonstrates that the joint effects of the gap opening and the exchange-spin splitting induced by the Ni substrate lead to the realization of the spin-polarized semiconductor-band structure in the graphene monolayer on a Ni(111) surface.

III. CONCLUSION

In summary, we demonstrate via spin-polarized STM measurements that the strong interaction between graphene and the Ni substrate generates a large gap in graphene and simultaneously leads to a relative shift between the majority- and minority-spin bands. Consequently, the graphene sheet on the Ni substrate exhibits a spin-polarized semiconductor-band structure even at room temperature.

ACKNOWLEDGMENTS

Yuchen Nie of the Experimental High School Attached to Beijing Normal University is acknowledged for experimental help. This work was supported by the National Natural Science Foundation of China (Grants No. 11674029, No. 11422430, and No. 11374035), the National Basic Research Program of China (Grants No. 2014CB920903 and No. 2013CBA01603), the program for New Century Excellent Talents in University of the Ministry of Education of China (Grant No. NCET-13-0054), the China Postdoctoral Science Foundation (Grant No. 212400207). L.H. also acknowledges support from the National Program for Support of Top-notch Young Professionals, support from "the Fundamental Research Funds for the Central Universities," and support from "Chang Jiang Scholars Program."

APPENDIX: PHYSICAL MECHANISM OF THE SPIN-POLARIZED GAP

The main mechanisms to induce a spin-polarized energy band in the graphene-Ni system may be attributed to (a) lattice deformations of graphene, (b) Rashba-type spin-orbit splitting, and (c) exchange splitting caused by magnetic atoms.

(a) Lattice deformations of graphene.

First-principles calculation illustrates that the increase of angle α between the basis vectors $\vec{a}_1$ and $\vec{a}_2$ can open up a band gap at K [15]. However, our atomic resolution STM images shown in Figs. 1(e) and S14 [20] exhibit a perfect triangular lattice with no deformation, which can thoroughly rule out this possibility.

(b) Rashba-type spin-orbit (SO) splitting.

Based on the effective-mass model [45], the spin-orbit coupling in graphene can be described as the sum of an intrinsic contribution and an extrinsic contribution. The intrinsic part is

$$H_{\mathrm{SO}}^{\mathrm{int}} = \lambda_i \psi^{\dagger} \sigma_z \tau_z s_z \psi .$$

The extrinsic part is

$$H_{\mathrm{SO}}^{\mathrm{ext}} = \lambda_R \psi^{\dagger} (\sigma_x \tau_z s_y - \sigma_y s_x) \psi ,$$

where the Pauli matrix σ_x, σ_y, and σ_z describe electronic states on the sublattice A or B of graphene, and τ_z describes states at K or K'. λ_i and λ_R are the strengths of the intrinsic SO coupling and the Rashba SO coupling.

The intrinsic SO splitting Δ_{SO} in freestanding graphene is approximately 0.02 meV [46]. An essential precondition to enhance the Rashba Δ_{SO} in graphene is to induce a substrate of high-nuclear charge, such as a Au (111) substrate ($\Delta_{\mathrm{SO}} = 13$ meV in a graphene-Au system) [46]. Nevertheless, the weight of Ni atoms are much lighter than Au atoms ($Z_{\mathrm{Ni}} = 28$ and $Z_{\mathrm{Au}} = 79$), thus a Ni substrate cannot be expected to induce a considerable Rashba Δ_{SO} [15,16,47], much smaller than the measured gap of approximately 40 meV in Figs. 2(a) and 3(c). In addition, Rashba splitting only induces spin splitting parallel to the film (see Fig. 4), while only the spin splitting perpendicular to the film can be detected in our experiment.

(c) Exchange splitting caused by magnetic atoms.

The most possible mechanism to open a similar-sized gap as that in our experiments in the graphene-Ni(111) system is that the strong chemical interaction between graphene and Ni results in an enormous sublattice asymmetry, which generates a large gap in graphene. And simultaneously, the exchange-splitting effect caused by magnetic atoms (Ni) leads to a relative shift between majority- and minority-spin bands. Consequently, the graphene sheet on the Ni substrate exhibits a spin-polarized gap with an energy of several tens of meV.

According to the tight-binding approximation, we can obtain the Hamiltonian near the Dirac points without SO coupling

$$\begin{aligned} H &= H_{\text{on-site}} + H_{\mathrm{hop}} + H_{\mathrm{ex}} + H_{\mathrm{asym}} \\ &= \sum_{i=1,2} \sum_{\alpha=\uparrow,\downarrow} \varepsilon c_{i\alpha}^{+} c_{i\alpha} + t \sum_{<i,j>} \sum_{\alpha=\uparrow,\downarrow} c_{i\alpha}^{+} c_{j\alpha} + \mathrm{H.c.} \\ &\quad + \sum_{i=1,2} \sum_{\alpha=\uparrow,\downarrow} \varepsilon_{\alpha} c_{i\alpha}^{+} c_{i\alpha} \sum_{i=1,2} \sum_{\alpha=\uparrow,\downarrow} (-1)^{i} \upsilon c_{i\alpha}^{+} c_{i\alpha} . \end{aligned}$$

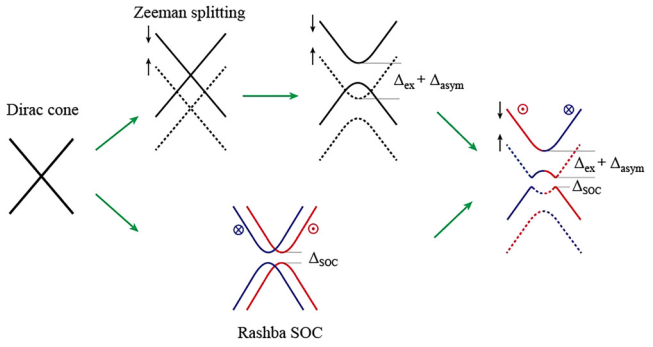

FIG. 4. Behavior of Dirac cone with Zeeman splitting and spin-orbit coupling. In this model, Δ_{ex}, Δ_{asym}, and Δ_{soc} represent the exchange-splitting energy, asymmetry potential of A and B sublattices, and SO splitting, respectively. Solid (dashed) black lines represent spin along the z direction. Red (blue) lines represent spin in the x-y plane.

Here, $H_{\text{on-site}}$, H_{hop}, H_{ex}, and H_{asym} represent the on-site energy term, the nearest-neighbor hopping term, the Zeeman-splitting term, and the asymmetry potential of A and B sublattices due to the Ni substrate. In the graphene-Ni(111) system, the carbon atoms of the A sublattice are mainly on top of the Ni atoms of the topmost atomic layer, while atoms of the B sublattice are mainly located above the hollow sites of the topmost atomic layer of Ni, as schematically shown in Fig. 1(f). The strong chemical interaction between graphene and Ni atoms results in the enormous asymmetric potential of approximately 150 meV, exhibiting a large band gap of approximately 300 meV. In addition, an obvious exchange-splitting effect is observed as a relative shift ($\Delta_{\mathrm{ex}} \sim 330$ meV) between the majority- and minority-spin bands, as shown in Fig. 2(b) and Fig. S15 [20]. This result coincides well with our spin-polarized STS measurements shown in Fig. 3(c).

Above all, we conclude that Ni has no obvious effect on the SO coupling in graphene. The combination of the enormous sublattice asymmetry and the exchange-splitting effect leads to a ferromagnetic-semiconducting state in the graphene-Ni system.

[1] C. Berger, Z. Song, X. Li, X. Wu, N. Brown, C. Naud, D. Mayou, T. Li, J. Hass, A. N. Marchenkov, E. H. Conrad, P. N. First, and W. A. de Heer, Electronic confinement and coherence in patterned epitaxial graphene, Science **312,** 1191 (2006).

[2] C. Tao, L. Jiao, O. V. Yazyev, Y.-C. Chen, J. Feng, X. Zhang, R. B. Capaz, J. M. Tour, A. Zettl, S. G. Louie, H. Dai, and M. F. Crommie, Spatially resolving edge states of chiral graphene nanoribbons, Nat. Phys. **7,** 616 (2011).

[3] Y. Y. Li, M. X. Chen, M. Weinert, and L. Li, Direct experimental determination of onset of electron-electron interactions in gap opening of zigzag graphene nanoribbons, Nat. Commun. **5**, 4311 (2014).

[4] G. Z. Magda, X. Jin, I. Hagymasi, P. Vancso, Z. Osvath, P. Nemes-Incze, C. Hwang, L. P. Biro, and L. Tapaszto, Room temperature magnetic order on zigzag edges of narrow graphene nanoribbons, Nature **514**, 608 (2014).

[5] Y. Zhang, S. Y. Li, H. Q. Huang, W. T. Li, J. B. Qiao, W. X. Wang, L. J. Yin, K. K. Bai, W. H. Duan, and L. He, Scanning Tunneling Microscopy of the π Magnetism of a Single Carbon Vacancy in Graphene, Phys. Rev. Lett. **117**, 166801 (2016).

[6] O. V. Yazyev and L. Helm, Defect-induced magnetism in graphene, Phys. Rev. B **75**, 125408 (2007).

[7] M. M. Ugeda, I. Brihuega, F. Guinea, and J. M. Gómez-Rodríguez, Missing Atom as a Source of Carbon Magnetism, Phys. Rev. Lett. **104**, 096804 (2010).

[8] M. M. Ugeda, D. Fernández-Torre, I. Brihuega, P. Pou, A. J. Martínez-Galera, R. Pérez, and J. M. Gómez-Rodríguez, Point Defects on Graphene on Metals, Phys. Rev. Lett. **107**, 116803 (2011).

[9] H. Gonzalez-Herrero, J. M. Gomez-Rodriguez, P. Mallet, M. Moaied, J. J. Palacios, C. Salgado, M. M. Ugeda, J.-Y. Veuillen, F. Yndurain, and I. Brihuega, Atomic-scale control of graphene magnetism by using hydrogen atoms, Science **352**, 437 (2016).

[10] R. R. Nair, M. Sepioni, I. Tsai, O. Lehtinen, J. Keinonen, A. V. Krasheninnikov, T. Thomson, A. K. Geim, and I. V. Grigorieva, Spin-half paramagnetism in graphene induced by point defects, Nat. Phys. **8**, 199 (2012).

[11] P. Wei, S. Lee, F. Lemaitre, L. Pinel, D. Cutaia, W. Cha, F. Katmis, Y. Zhu, D. Heiman, J. Hone, J. S. Moodera, and C.-T. Chen, Strong interfacial exchange field in graphene/EuS heterostructure, Nat. Mater. **15**, 711 (2016).

[12] Z. Wang, C. Tang, R. Sachs, Y. Barlas, and J. Shi, Proximity-Induced Ferromagnetism in Graphene Revealed by the Anomalous Hall Effect, Phys. Rev. Lett. **114**, 016603 (2015).

[13] W. Han, R. K. Kawakami, M. Gmitra, and J. Fabian, Graphene spintronics, Nat. Nanotechnol. **9**, 794 (2014).

[14] P. A. Khomyakov, G. Giovannetti, P. C. Rusu, G. Brocks, J. van den Brink, and P. J. Kelly, First-principles study of the interaction and charge transfer between graphene and metals, Phys. Rev. B **79**, 195425 (2009).

[15] S. Abdelouahed, A. Ernst, J. Henk, I. V. Maznichenko, and I. Mertig, Spin-split electronic states in graphene: Effects due to lattice deformation, Rashba effect, and adatoms by first principles, Phys. Rev. B **82**, 125424 (2010).

[16] O. Rader, A. Varykhalov, J. Sanchez-Barriga, D. Marchenko, A. Rybkin, A. M. Shikin. Is There a Rashba Effect in Graphene on *3d* Ferromagnets? Phys. Rev. Lett. **102**, 057602 (2009).

[17] Y. Zhang, L. Gomez, F. N. Ishikawa, A. Madaria, K. Ryu, C. Wang, A. Badmaev, and C. Zhou, Comparison of graphene growth on single-crystalline and polycrystalline Ni by chemical vapor deposition, J. Phys. Chem. Lett. **1**, 3101 (2010).

[18] Q. Yu, J. Lian, S. Siriponglert, H. Li, Y. P. Chen, and S. Pei, Graphene segregated on Ni surfaces and transferred to insulator, Appl. Phys. Lett. **93**, 113103 (2008).

[19] K. S. Kim, Y. Zhao, H. Jang, S. Y. Lee, J. M. Kim, K. S. Kim, J. H. Ahn, P. Kim, J. Y. Choi, and B. H. Hong, Large-scale pattern growth of graphene films for stretchable transparent electrodes, Nature **457**, 706 (2009).

[20] See Supplemental Material at http://link.aps.org/supplemental/10.1103/PhysRevApplied.10.054043 for methods, more STM images, STS spectra, and details of the calculations.

[21] A. C. Ferrari, J. C. Meyer, V. Scardaci, C. Casiraghi, M. Lazzeri, F. Mauri, S. Piscanec, D. Jiang, K. S. Novoselov, S. Roth, and A. K. Geim, Raman Spectrum of Graphene and Graphene Layers, Phys. Rev. Lett. **97**, 187401 (2006).

[22] Y. Zhang, V. W. Brar, F. Wang, C. Girit, Y. Yayon, M. Panlasigui, A. Zettl, and M. F. Crommie, Giant phonon-induced conductance in scanning tunnelling spectroscopy of gate-tunable graphene, Nat. Phys. **4**, 627 (2008).

[23] H. W. Kim, W. Ko, J. Ku, I. Jeon, D. Kim, H. Kwon, Y. Oh, S. Ryu, Y. Kuk, S. W. Hwang, and H. Suh, Nanoscale control of phonon excitations in graphene, Nat. Commun. **6**, 7528 (2015).

[24] F. D. Natterer, Y. Zhao, J. Wyrick, Y. Chan, W. Ruan, M. Chou, K. Watanabe, T. Taniguchi, N. B. Zhitenev, and J. A. Stroscio, Strong Asymmetric Charge Carrier Dependence in Inelastic Electron Tunneling Spectroscopy of Graphene Phonons, Phys. Rev. Lett. **114**, 245502 (2015).

[25] L. J. Yin, Y. Zhang, J. B. Qiao, S. Y. Li, and L. He, Experimental observation of surface states and Landau levels bending in bilayer graphene, Phys. Rev. B **93**, 125422 (2016).

[26] L. J. Yin, S. Y. Li, J. B. Qiao, J. C. Nie, and L. He, Landau quantization in graphene monolayer, Bernal bilayer, and Bernal trilayer on graphite surface, Phys. Rev. B **91**, 115405 (2015).

[27] G. Giovannetti, P. A. Khomyakov, G. Brocks, V. M. Karpan, J. van den Brink, and P. J. Kelly, Doping Graphene with Metal Contacts, Phys. Rev. Lett. **101**, 026803 (2008).

[28] K. K. Bai, Y. C. Wei, J. B. Qiao, S. Y. Li, L. J. Yin, W. Yan, J. C. Nie, and L. He, Detecting giant electron-hole asymmetry in a graphene monolayer generated by strain and charged-defect scattering via Landau level spectroscopy, Phys. Rev. B **92**, 121405(R) (2015).

[29] J. Tian, H. Cao, W. Wu, Q. Yu, N. P. Guisinger, and Y. P. Chen, Graphene induced surface reconstruction of Cu, Nano Lett. **12**, 3893 (2012).

[30] B. Kiraly, E. V. Iski, A. J. Mannix, B. L. Fisher, M. C. Hersam, and N. P. Guisinger, Solid-source growth and atomic-scale characterization of graphene on Ag(111), Nat. Commun. **4**, 1965 (2013).

[31] D. Xiao, W. Yao, and Q. Niu, Valley-Contrasting Physics in Graphene: Magnetic Moment and Topological Transport, Phys. Rev. Lett. **99**, 236809 (2007).

[32] G. Giovannetti, P. A. Khomyakov, G. Brocks, P. J. Kelley, and J. van den Brink, Substrate-induced band gap in graphene on hexagonal boron nitride: Ab initio density functional calculations, Phys. Rev. B **76**, 073103 (2007).

[33] Z. G. Chen, Z. Shi, W. Yang, X. Lu, Y. Lai, H. Yan, F. Wang, G. Zhang, and Z. Li, Observation of an intrinsic bandgap and Landau level renormalization in graphene/boron-nitride heterostructures, Nat. Commun. **5**, 4461 (2014).

[34] W. Kohn, and L. J. Sham, Self-consistent equations including exchange and correlation effects. Phys. Rev. **140**, A1133 (1965).
[35] G. Kresse and J. Furthmuller, Efficiency of ab-initio total energy calculations for metals and semiconductors using a plane-wave basis set, Comput. Mater. Sci. **6**, 15 (1996).
[36] J. P. Perdew and A. Zunger, Self-interaction correction to density-functional approximations for many-electron systems, Phys. Rev. B **23**, 5048 (1981).
[37] P. E. Blochl, Projector augmented-wave method, Phys. Rev. B **50**, 17953 (1994).
[38] M. Weser, Y. Rehder, K. Horn, M. Sicot, M. Fonin, A. B. Preobrajenski, E. N. Voloshina, E. Goering, and Yu. S. Dedkov, Induced magnetism of carbon atoms at the graphene/Ni(111) interface, Appl. Phys. Lett. **96**, 012504 (2010).
[39] A. Miyashita, M. Maekawa, K. Wada, A. Kawasuso, T. Watanabe, S. Entani, and S. Sakai, Spin polarization of graphene and *h*-BN on Co(0001) and Ni(111) observed by spin-polarized surface positronium spectroscopy, Phys. Rev. B **97**, 195405 (2018).
[40] M. Bode, Spin-polarized scanning tunnelling microscopy, Rep. Prog. Phys. **66**, 523 (2003).
[41] R. Wiesendanger, Spin mapping at the nanoscale and atomic scale, Rev. Mod. Phys. **81**, 1495 (2009).
[42] H. Chen, W. Xiao, X. Wu, K. Yang, and H. J. Gao, Electrochemically etched Ni tips in a constant-current mode for spin-polarized scanning tunneling microscopy, Vac. Sci. Technol. B **32**, 061801 (2014).
[43] M. V. Rastei and J. P. Bucher, Spin polarized tunnelling investigation of nanometer Co clusters by means of a Ni bulk tip, J. Phys.: Condens. Matter **18**, L619 (2006).
[44] L. V. Dzemiantsova, M. Karolak, F. Lofink, A. Kubetzka, B. Sachs, K. von Bergmann, S. Hankemeier, T. O. Wehling, R. Fromter, H. P. Oepen, A. I. Lichtenstein, and R. Wiesendanger, Multiscale magnetic study of Ni(111) and graphene on Ni(111), Phys. Rev. B **84**, 205431 (2011).
[45] C. L. Kane and E. J. Mele, Quantum Spin Hall Effect in Graphene, Phys. Rev.Lett. **95**, 226801 (2005).
[46] M. Gmitra, S. Konschuh, C. Ertler, C. Ambrosch-Draxl, and J. Fabian, Band-structure topologies of graphene: Spin-orbit coupling effects from first principles, Phys. Rev. B **80**, 235431 (2009).
[47] D. Marchenko, A. Varykhalov, M. R. Scholz, G. Bihlmayer, E. I. Rashba, A. Rybkin, A. M. Shikin, and O. Rader, Giant Rashba splitting in graphene due to hybridization with gold, Nat. Commun. **3**, 1232 (2012).